Supporting Information

Fanelli et al. 10.1073/pnas.1007647107

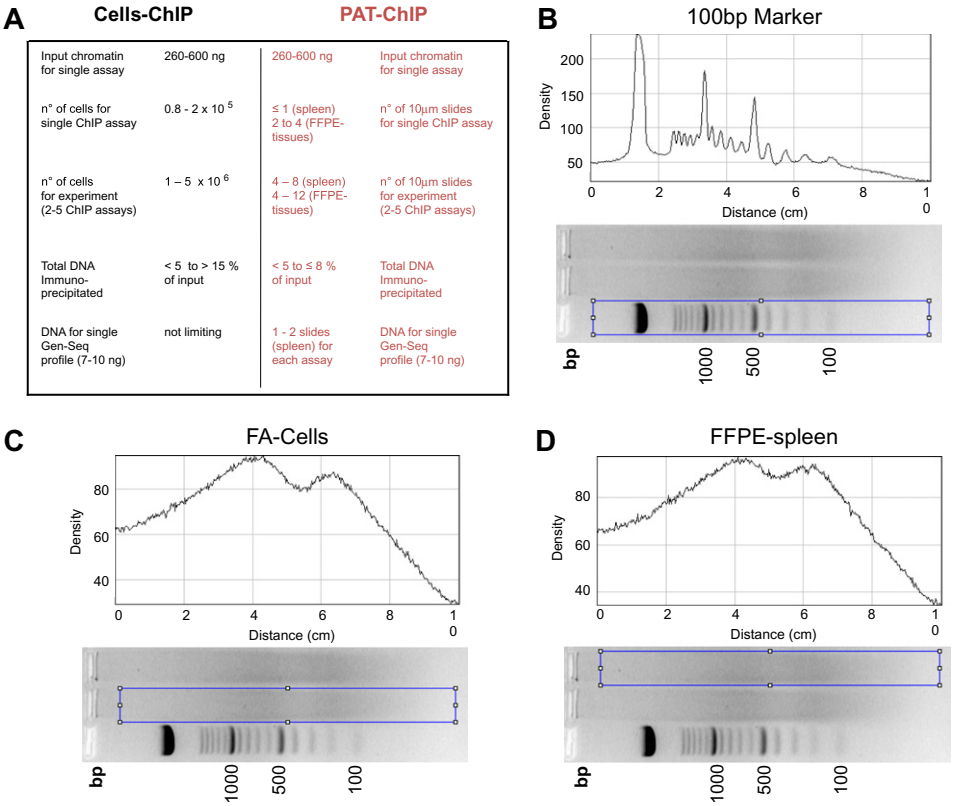

Fig. S1. Cells-ChIP and pathology tissue–ChIP (PAT-ChIP) technical summary and densitometric analysis. (*A*) Summary of the most relevant technical information regarding both canonical Cells-ChIP and PAT-ChIP procedures carried out in this study. DNA obtained from FA-Cells or FFPE-spleen, representative of the ChIP starting material (Input), was separated by agarose gel electrophoresis and stained by ethidium bromide. Densitometric plot profiles are reported for the corresponding samples of DNA (blu rectangle): (*B*) 100 bp marker, (*C*) FA-Cells, and (*D*) FFPE-Spleen. Densitometric analysis was performed by using National Institutes of Health Image 64J software.

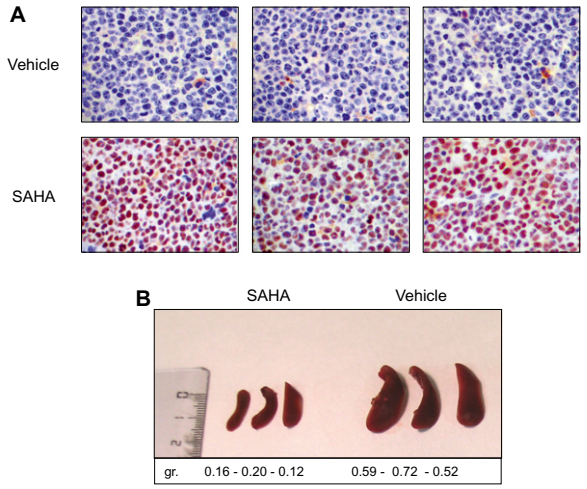

Fig. S2. In vivo response of acute promyelocytic leukemia mice to suberoylanilide hydroxamic acid (SAHA) treatment. (*A*) Immunohistochemical analysis of the histone H4 acetylation levels of spleen sections derived from leukemic mice, treated or untreated for 4 d with SAHA (150 mg/kg per die). (*B*) Prevented splenomegaly, of the same spleens, is shown with the corresponding weight in grams.

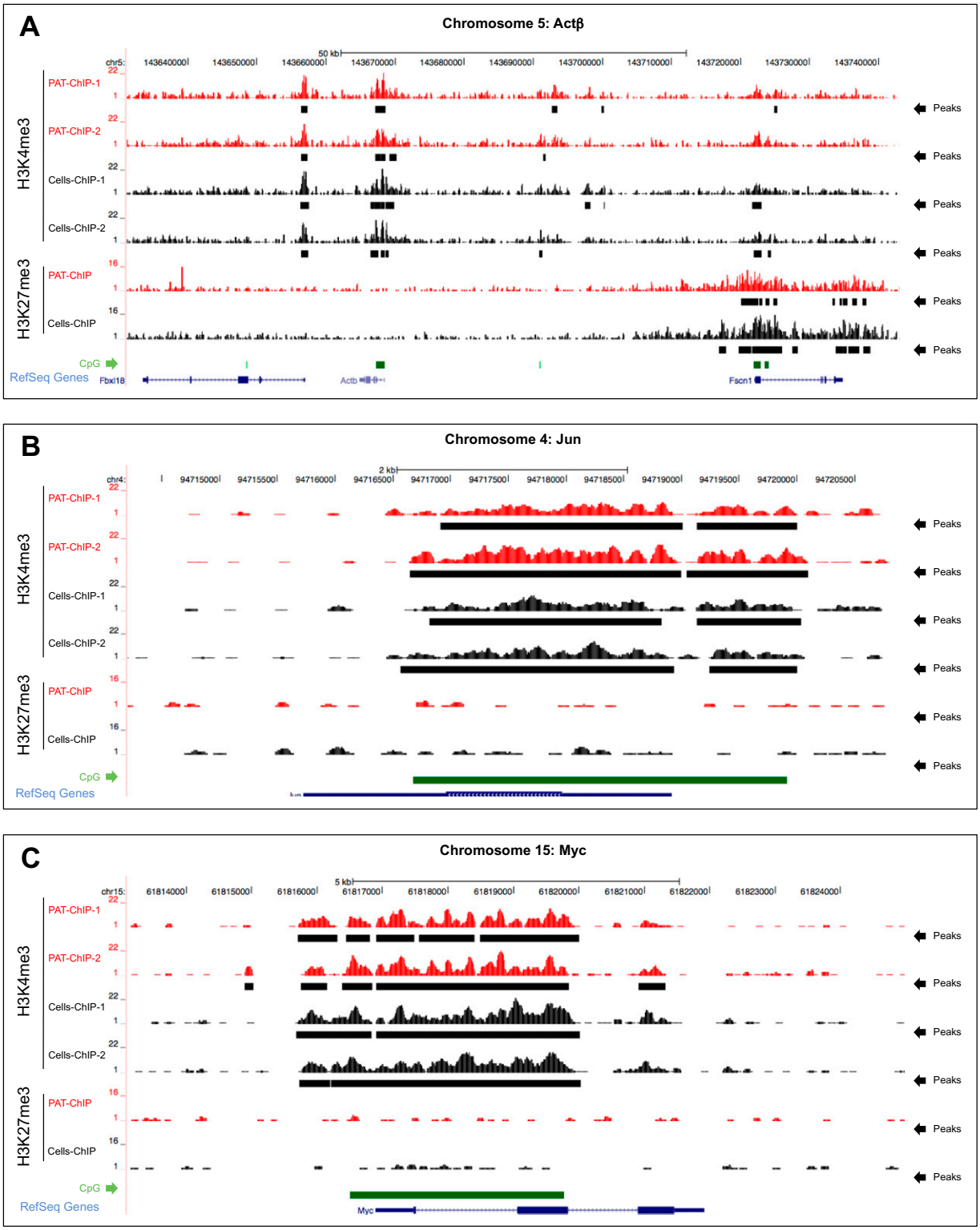

Fig. S3. Additional screenshots as examples of H3K4me3 and H3K27me3 immunoselections performed by both Cells-ChIP and pathology tissue–ChIP (PAT-ChIP) procedures: (*A*) Actβ, (*B*) Jun, and (*C*) Myc genomic loci.

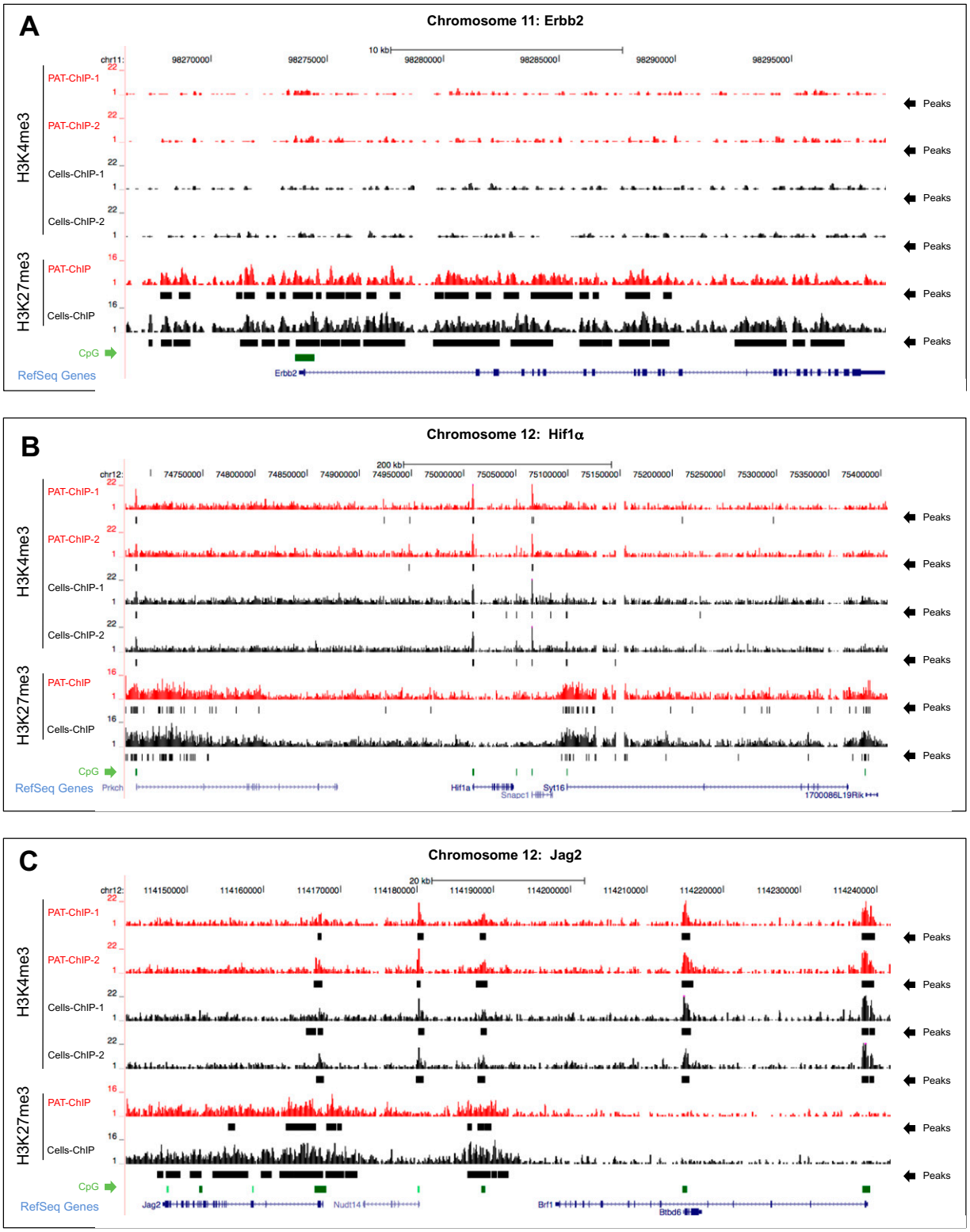

Fig. S4. Additional screenshots as examples of H3K4me3 and H3K27me3 immunoselections performed by both Cells-ChIP and pathology tissue–ChIP (PAT-ChIP) procedures: (*A*) Erbb2, (*B*) Hif1α, and (*C*) Jag2 genomic loci.

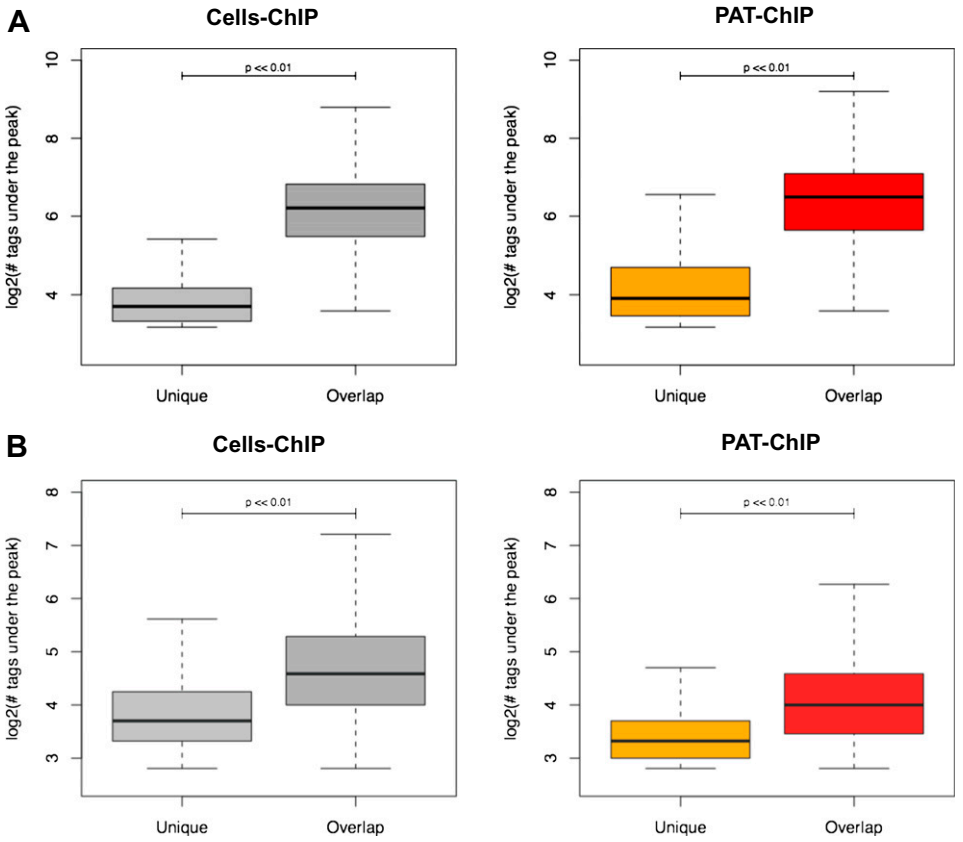

Fig. S5. Distribution of peaks from ChIP-Seq experiments. The boxplots show the distributions of the number of tags (reads) constituting either overlapping or unique peaks in both Cells-ChIP and pathology tissue–ChIP (PAT-ChIP) datasets obtained by (*A*) H3K4me3 and (*B*) H3K27me3 immunoselection. To normalize their distributions the numbers of tags are expressed as their logarithm. Unpaired one-tailed Mann–Whitney test was performed to test whether the distribution of the overlapping peaks shows a significantly higher median than the unique ones.

Table S1. Correlation coefficient and statistical analysis of Cells-ChIP vs. pathology tissue–ChIP (PAT-ChIP) shown in Fig. 2

Table S1 (DOC)

(*A*) Pearson product-moment correlation coefficient was calculated considering the experiment reported in Fig. 2*A* ($P < 0.005$). (*B*) Pearson product-moment correlation coefficient was calculated considering a total of 12 ChIP assays and 180 quantitative PCR amplifications of the experiment reported in Fig. 2*B* ($P < 0.003$). Fisher's transformation was applied to improve the normal approximation of the data distribution of the correlation coefficient. *P* value was evaluated by using the Fisher's transformation of the sample correlation coefficient. (*C*) List of primers used to perform the quantitative PCR assays shown in Fig. 2 *A* and *B* and Fig. 3 B–E and H–L.

Dataset S1. Complete list and relative features regarding the peaks obtained, by H3K4me3 immunoselection, by Cells-ChIP and pathology tissue–ChIP (PAT-ChIP) (each in duplicate)

Dataset S1 (XLS)

Dataset S2. Analysis of the overlapping between Cells-ChIP and pathology tissue–ChIP (PAT-ChIP) datasets with respect to peaks distribution, RefSeqs TSS, and CpG island

Dataset S2 (XLS)

Dataset S3. Complete list and relative features regarding the peaks obtained, by H3K27me3 immunoselection, by Cells-ChIP and pathology tissue–ChIP (PAT-ChIP)

Dataset S3 (XLS)